R. & M. No. 2748
(11,429, 12,237)
A.R.C. Technical Report

MINISTRY OF SUPPLY

AERONAUTICAL RESEARCH COUNCIL
REPORTS AND MEMORANDA

The Measurement of the Overall Drag of an Aircraft at High Mach Numbers

By

D. J. HIGTON, A.M.I.Mech.E., A.F.R.Ae.S.,
R. H. PLASCOTT, B.Sc. (Eng.),
and
D. A. CLARKE, B.Sc. (Eng.), A.C.G.I.

LONDON: HER MAJESTY'S STATIONERY OFFICE
1953
SIX SHILLINGS NET

The Measurement of the Overall Drag of an Aircraft at High Mach Numbers

By

D. J. HIGTON, A.M.I.Mech.E., A.F.R.Ae.S.,
R. H. PLASCOTT, B.Sc. (Eng.),
and
D. A. CLARKE, B.Sc (Eng.), A.C.G.I.

COMMUNICATED BY THE PRINCIPAL DIRECTOR OF SCIENTIFIC RESEARCH (AIR), MINISTRY OF SUPPLY

Reports and Memoranda No. 2748*
January, 1949

Summary.—This report describes the technique which has been developed to measure the overall drag of an aircraft at high Mach numbers in both level flight and dives. It shows how improvements have been made both in flight and tunnel technique so that comparisons between full-scale and model tests have now become possible.

Flight results from *Meteor IV* aircraft show close agreement between drag measured in level flight and in dives and later tests compare well with high-speed wind-tunnel measurements on a 1/12th scale model.

1. *Introduction.*—The effect of compressibility on the overall drag of an aircraft was first measured in flight some years ago by recording speed and altitudes during sustained dives[1]. These early tests were of great value, since they provided the first measurement of the drag rise at full-scale Reynolds numbers in free air. They were, however, subject to considerable inaccuracies and, although a substantial improvement was effected by the introduction of a longitudinal accelerometer[2,3] which provided a direct record of the aircraft's acceleration during the dives, the errors involved were still sufficiently large to limit the usefulness of the results.

Attempts have therefore been made to improve the technique and it has now been found that by giving sufficient attention to detail, together with some minor refinements, a very good standard of accuracy can be achieved in the measurement of drag when diving.

Corresponding improvements in technique were made at about the same time in high-speed wind-tunnel testing. Up to that time, models were large, having wing spans of about 6 ft, and were supported on three struts, one attached to each wing and one to the rear fuselage. Corrections for wind-tunnel blockage and for strut interference were large and of doubtful validity. Models were therefore reduced to about half their former size, and were supported from the rear. This enabled tests to be made at higher Mach numbers, while reducing the wind-tunnel blockage corrections and practically eliminating all support interference.

It was considered that it was now possible to make a true comparison of flight and wind-tunnel drag measurements and therefore wind-tunnel tests were undertaken on an accurate 1/12 scale model of the aircraft used in the flight measurements (*Meteor IV*, EE. 454).

*Revised version of { R.A.E. Report Aero. 2241, received 22nd April, 1948.
R.A.E. Report Aero. 2309, received 19th March, 1949.

As the flight tests had been carried out at medium altitudes, the lift coefficients at which the measurements were made had been low and, in order to extend the comparison to higher lift coefficients, further flight tests were undertaken. At this time the aircraft used previously was no longer available and the measurements were made on another *Meteor IV* (VT. 108), although the shorter span of this aircraft slightly reduced the value of the comparison.

2. *Description of the Aircraft Instrumentation.*—The two aircraft used in these flight tests were *Meteor IV* EE. 454 and *Meteor IV* VT. 108 (Fig. 1 and Table 1).

(a) *Meteor IV* EE. 454.—This was one of the first aircraft of its type, and retained the ' full-span ' wings of the preceding marks. Otherwise it was externally identical with a standard *Meteor IV*; the gun-blast tubes were faired over to the fuselage lines.

An incidence vane and an outside air thermometer were fitted to the aircraft. These instruments are very small and their influence on the total drag would be negligible.

The surface finish of the aircraft was not particularly good and towards the end of the tests there were regions where the paint work had broken away from the skin, particularly on the fuselage and nacelles, due to the large amount of flying which was done at these high Mach numbers.

The aircraft was fitted with an automatic observer containing the following instruments:—airspeed indicator, two sensitive altimeters (connected together by a length of calibrated fine bore tubing for the purpose of determining the lag corrections in high-speed dives as outlined in R. & M. 2352[4]), normal accelerometer, clock, two engine speed indicators, two jet-pipe pitot pressure gauges, two jet-pipe temperature indicators, an outside air temperature indicator, and a Desynn indicator for the measurement of longitudinal acceleration. A Machmeter and a direct reading normal accelerometer were fitted in the cockpit.

The standard leading-edge pitot-static head position was used and the A.S.I. and the altimeters in the auto-observer were connected to the aircraft pitot-static system in the normal manner. There was a single total-head tube in each jet-pipe situated at the standard test-bed position, *i.e.*, at 34 in. from the final nozzle and $2\frac{1}{2}$ in. from the wall of the jet-pipe; the jet-pipe pitot pressures were measured relative to the aircraft static pressure.

These instruments in the auto-observer were photographed by a robot camera controlled by the pilot who could select either single shots or automatic, where photographs would be taken continuously at predetermined intervals. A four-channel continuous-trace Desynn recorder was also fitted, providing continuous records of the longitudinal acceleration, elevator angle, rudder angle and for-and-aft stick force. The last three channels together with vibrographs were used to investigate stability characteristics at high Mach numbers during other tests. This instrument was equipped with a time base to enable direct correlation between the continuous records and the automatic observer readings to be made.

The longitudinal accelerometer was mounted parallel to the fuselage datum and very near to the centre of gravity of the aircraft. This instrument employed the principle of the Barnes type accelerometer. The mechanism consists of a spring-restrained weight sliding between two rotating rollers. The displacement of this weight is transmitted by means of a micro-Desynn to a Desynn receiver on the instrument panel and to the continuous-trace recorder mentioned above. The damping of the accelerometer could be adjusted over a small range by increasing or decreasing the friction between the weight and the rollers. This accelerometer was built by the R.A.E. Instruments Dept. Its range was $-0{\cdot}2g$ to $+0{\cdot}95g$ and its natural frequency $3{\cdot}5$ c.p.s. The type of longitudinal acceleration, which is recorded in drag measurement tests, builds up and diminishes very gradually with an average rate of approximately $0{\cdot}01g$ per sec. Some typical time histories are given in Figs. 2a, 2b, and 2c, showing the variation in longitudinal acceleration during the dives. In view of the slowly changing acceleration it is more desirable to obtain steady readings than to achieve very rapid response. It was found that to satisfy this requirement the damping was at its best when at about the critical value, *i.e.*, the friction between

the weight and the rollers was adjusted so that, when the weight was deflected, it returned to its original position in the minimum time without overshooting. The calibration of the accelerometer was frequently checked and care was taken to ensure that the damping remained at about the optimum during the tests.

(b) *Meteor IV* VT. 108.—This aircraft was a standard production version fitted with the modified clipped wings and a pressure cabin. The gun-blast tubes were faired over with shaped wooden fairings to the fuselage lines and an outside air thermometer was fitted beneath the fuselage.

The instrumentation in this aircraft was identical to that of *Meteor IV* EE. 454 except that the longitudinal accelerometer was omitted as all the measurements were made in level flight.

No special attention was given to the surface finish of the aircraft apart from seeing that it was clean before flight. The paintwork, joints, rivets and leaks were of the standard production quality and no attempt was made to improve them. The condition of the aircraft, however, compared favourably with that of the other aircraft.

3. *Description of the Tests and Technique.*—3.1. *Meteor IV* EE. 454.—The position errors on the pitot-static system were measured by the aneroid method. The measured sea level position error curve, together with the calculated altitude curves[5] are given in Fig. 3.

The results of R. & M. 2446[6] provided a curve of drag coefficient at zero lift against Mach number for this particular aircraft, measured in level flight up to a Mach number of 0·81.

Considerable time had elapsed, however, since those results were obtained and the surface finish of the aircraft had deteriorated badly. It was therefore considered essential to measure the drag coefficients again in level flight to provide a true basic drag curve.

These preliminary level flight tests were made at 25,000 ft over the whole speed range up to a Mach number of 0·81. The engine thrusts corresponding to each speed were measured using the method given in Appendix I and the overall drag coefficients were computed by equating the total thrust from the engines to the total aircraft drag.

In the previous tests on this aircraft (R. & M. 2446[6]) it was deduced that the effective induced drag factor K was 1·10 up to the start of the drag rise. This value was used in calculating the profile drag coefficients of the present tests for comparison with the results of R. & M. 2446[6]. However, for comparison with the results obtained later on *Meteor IV* VT. 108 and the tunnel measurements, the results were analysed using the more accurate values of K determined in the measurements on *Meteor IV* VT. 108.

In view of the Reynolds number effects which were shown to be present during the earlier work (R. & M. 2446[6]) it was desirable to obtain the results from the dives in the region of the height at which the level flight tests were made, *i.e.*, 25,000 ft, in order to provide a direct comparison. The pilots therefore endeavoured to reach the peak Mach numbers in their dives at approximately this altitude.

The dives were made over a range of engine speeds from almost full throttle (14,000 r.p.m.) down to 10,000 r.p.m.; the dives with the engines partially throttled were made in an attempt to simulate the earlier dive tests on a *Meteor I*[3] by using similar thrusts and mass flows as in those tests. This technique covered a range of angles of dive from 10 to 40 deg, with rates of descent from 5,000 to 30,000 ft/min.

The pilots were instructed to take care to avoid any sideslip during the dives in order to minimise the scatter of the measurements due to piloting errors.

The overall drag of the aircraft in the dive was calculated using the method given in Appendix II, the aircraft weight being known from fuel content readings taken by the pilot and the engine thrusts being determined as in the level flight case.

3.2. *Meteor IV* VT. 108.—All the measurements on this aircraft were made in level flight. The aircraft was equipped with a pressure cabin enabling results to be obtained at greater altitudes than previously (up to 47,000 ft) and therefore made possible drag measurements at high Mach numbers at much greater lift coefficients than in the tests on the other aircraft.

In order to facilitate comparison with the wind-tunnel measurements, which are presented as curves of overall drag coefficient with Mach number for constant values of lift coefficient, the flight tests were conducted so that the full-scale results could be produced in the same manner. This involved making the measurements at constant equivalent airspeed, the Mach number range being covered by varying the altitude. The pilot was given conditions to fly to which took account of the position and compressibility errors and to which he made a final correction depending on the amount of fuel in the aircraft.

This technique proved to be satisfactory and curves were obtained at mean lift coefficients of 0·06, 0·24 and 0·33. Small changes in lift coefficient were, however, present due to piloting inaccuracies and account for some of the experimental scatter.

The jet-pipe method of measuring the engine thrust already mentioned was used and, as the measurements were made in level flight, the overall drag of the aircraft was computed by equating it to the measured nett thrust.

The range of Reynolds number covered in these tests was from 12 to 45 $\times$ 10^6, based on the mean wing chord. It so happens that using the technique described above the range of Reynolds number covered at any particular value of C_L is small but there is a large variation across the C_L range at a constant Mach number. It must therefore be remembered that the effective induced drag factor K, which has been determined from these results for comparison with the wind-tunnel measurements, includes a Reynolds number effect, the magnitude of which is unknown.

4. *Results.*—4.1. *Meteor IV* EE. 454.—It was found from the preliminary drag measurements made in level flight on this aircraft that the drag at zero lift was, if anything, slightly higher than the results obtained in the earlier tests on this aircraft, as shown in Fig. 4.

The surface condition of the aircraft, when used for those early tests, was of a fairly high standard although probably not sufficiently good to have achieved an appreciably far back transition point. The prolonged flying at high Mach numbers between the two sets of tests on other experiments caused a severe deterioration in surface condition which possibly accounts for the slightly higher drag in the present tests.

The profile-drag coefficients measured in all of the dives irrespective of engine conditions or angle of dive are presented in Fig. 5. The curve obtained from the level-flight measurements is also given in this figure and is in extremely close agreement with the dive results. This is contrary to the impression gained when comparing these results with the earlier, less accurate dive tests on a *Meteor I* fitted with long nacelles[3] (Fig. 6).

The scatter of the experimental points from these present diving tests is much less than in the earlier tests; this has mainly been achieved by paying particular attention to the accelerometer damping and also by using apparatus giving a continuous record of the longitudinal acceleration rather than taking 'spot' readings from automatic observer photographs.

Comparing the results of the present dive tests with the earlier ones we see that in addition to the improved accuracy of the present results there is a marked difference between the curves obtained. The latest results in fact tend to be a lower envelope of the whole of the earlier experimental results (Fig. 6).

Although the external shapes of the aircraft used in each set of tests were almost the same, the Derwent V units of the *Meteor IV* aircraft consumed much larger quantities of air under normal operating conditions than the W2.700 units of the *Meteor I*. The tests made at 14,000 r.p.m. covered a mass flow range of 36 to 45 lb/sec from start to finish of the dive while

those made at the lower engine speeds to simulate the *Meteor I* dive tests covered a mass flow range from 14 to 26 lb/sec. This change in air flow conditions through the nacelles, however, made no measurable difference to the values of the drag coefficients obtained (Fig. 5).

A possible explanation of the difference is that the slight change in nacelle shape on the *Meteor IV* to accommodate the larger diameter jet-pipes (4 in. greater in diameter than on the *Meteor I*) may have the same effect as a further increase in the fineness ratio of the nacelle.

There was no evidence of the ' hysteresis ' effect in the drag curve observed in other tests; *e.g.*, the tests on *Spitfire IX*[7] which showed that when the Mach number was decreasing the drag coefficients were apparently higher than when the Mach number was increasing, thus forming two distinct curves.

4.2. *Meteor IV* VT. 108.—The results of the measurements on this aircraft are presented in Fig. 7. The drag curve obtained in the previous tests has been corrected using the more accurate values of the induced drag factor determined in these latter tests (Fig. 12) and is also shown in Fig. 7 for comparison. The agreement between the two sets of measurements is so close that it is impossible to distinguish any difference in the drag coefficients at zero lift.

These results will be discussed in detail when compared with the wind-tunnel measurements.

5. *Description of Wind-Tunnel Tests.*—5.1. *Description of Model and Support System.*—The 1/12th scale model representing *Meteor IV* EE. 454 was made of laminated teak with a smooth, polished Phenoglaze finish and with Tufnol trailing edges. Flow through the nacelles was not represented and the control gaps were faired in. The only major difference between aircraft and model was the fairing of the nacelles at entry and exit. A photograph of the model is shown in Fig. 8.

The aft cantilever strut support system described in Ref. 8 was modified for drag measurement. A schematic diagram of the layout is presented in Fig. 9. The sting supporting the model was fixed at the rear to a tube hanging on two sets of links from an outer housing. Behind the rear links the tube was connected to this housing by a steel spring. A drag force on the model extended the spring and the movement was measured on an electro-magnetic balance. The housing was encased in an outer tube, which was supported by wires from the tunnel walls. A full description of the drag balance and its calibration is given in Ref. 9.

To restrict vertical vibration of the model a weight was suspended in an oil pot from a point about 4 in. aft of the wing root trailing edge.

Lift was measured by strain-gauges placed at two stations on the sting.

5.2. *Wind-Tunnel Programme.*—Drag, lift, tube incidence, tube air pressure and wind-tunnel wall pressures near the model were measured at approximately 1 deg intervals of incidence up to $C_L = 0{\cdot}3$ over a range of Mach number from $0{\cdot}50$ to $0{\cdot}90$. Tunnel choking occurred at $M = 0{\cdot}91$.

Tests to determine the drag of the faired sting and damping wire were made at the same incidences and Mach numbers with the model removed from the sting and replaced by an ellipsoidal fairing fitted over its nose; the damping wire was attached at the same position as in the presence of the model.

The Reynolds number was kept constant throughout at $R = 0{\cdot}43 \times 10^6$ based on the mean wing chord of the model.

5.3. *Corrections to Wind-Tunnel Results.*—It was found that the effect of the difference of tube air pressure between the model test and the faired sting test was negligible when expressed as a drag coefficient based on wing area.

The model drag was therefore corrected for support and damping wire interference by subtracting from the measured value the drag measured in the faired sting test. The accuracy of this correction depends on the following assumptions:—

(a) The drag of the fairing over the part of the sting normally inside the model is small. No reliable measured value is available but the skin friction drag of the fairing was calculated to be about $0{\cdot}002$ in C_D.

(b) The presence of the sting does not affect the air flow over the model.

(c) If the sting had not been present, the mean pressure over the rear cross-section of the fuselage would have been equal to the static pressure in the undisturbed stream ahead of the model.

Little information is available on how far the second and third assumptions are justified but it is probable that the effect of the third is small since a change of C_p of $0{\cdot}1$ at the rear of the fuselage will only produce a change of $0{\cdot}0008$ in model C_D. Assuming that the second assumption is justified for lack of contrary evidence, then the method gives model drag coefficients which are underestimated by about $0{\cdot}002$.

The method of correction for blockage was as follows. The total peak velocity increment at the walls due to the presence of the model was found from the wall pressures and was assumed to be equal to $(\varepsilon_W + 2\varepsilon_S)$ where ε_S is the increment of velocity at the model due to solid blockage and ε_W that due to the wake blockage. The latter was found from the measured drag values in the usual way[10] and hence it was possible to derive ε $(= \varepsilon_S + \varepsilon_W)$ and the correction to the Mach number.

$$\frac{\Delta M}{M} = (1 + \tfrac{1}{5} M^2)\, \varepsilon \cdot$$

The following table gives the values of ΔM for various values of uncorrected Mach number.

M	$0{\cdot}7$	$0{\cdot}8$	$0{\cdot}85$	$0{\cdot}875$
ΔM	0	$0{\cdot}005$	$0{\cdot}009$	$0{\cdot}015$

The blockage correction to $\frac{1}{2}\rho V^2$ was very small and was not applied.

6. *Comparison of Flight and Wind-Tunnel Measurements.*—The results of the wind-tunnel measurements are presented in Fig. 10 and a comparison is made with the results of the flight tests in Fig. 11.

At $C_L = 0$ both the wind-tunnel and flight results show an increase of drag coefficient of $0{\cdot}012$ from $M = 0{\cdot}50$ to $M = 0{\cdot}82$. However, whereas the drag as measured in flight starts to rise at $M = 0{\cdot}70$, in the wind tunnel the rise starts gradually and at a lower Mach number. Although this small difference is at the limit of the experimental accuracy, it is possibly caused by the difference in Reynolds number. No flight results at present available show a rise of drag at these moderate Mach numbers but the effect has been noted in wind-tunnel tests on several other models. In some cases, the effect has been found to vary with Reynolds number. It is possible that in the wind-tunnel tests a forward movement of the transition position or the development of a laminar separation results from an increase in Mach number, thus giving an early drag rise.

The agreement between the wind-tunnel and flight measurements on the shape of the drag curve is also good at the higher lift coefficients. The flight results show a more gradual rise, which starts at a lower Mach number.

The fairly close agreement in the drag rise between model and full-scale results in these tests should not be interpreted as applying necessarily for other aircraft designs. The boundary-layer effects mentioned above are of course dependent on the particular wing pressure distribution

and may be aggravated by any marked spanwise flow, such as is encountered on highly tapered or swept wings. There is some evidence that the early drag rise is more apparent in model tests on such wings.

The agreement in the absolute values of C_D at $C_L = 0$ (*e.g.*, at $M = 0{\cdot}5$, model $C_D = 0{\cdot}017$ and full-scale $C_D = 0{\cdot}016$) is interesting but probably has little meaning. As explained in section 5.3, the wind-tunnel results should probably be increased by $0{\cdot}002$ in C_D at all Mach numbers. The resulting difference of $0{\cdot}003$ in C_D at $M = 0{\cdot}5$ would be no more than might be expected in view of the difference in Reynolds number and surface finish. The apparent improvement in agreement of the absolute value of C_D at the higher lift coefficients is due of course to the increased induced-drag contribution resulting from the lower aspect ratio of the full-scale aircraft.

Fig. 12 presents a comparison of the value of the effective induced-drag factor K calculated from the relation

$$C_D = C_{D0} + \frac{KC_L^2}{\pi A} \cdot$$

At $M = 0{\cdot}5$ the flight value is $1{\cdot}3$, the corresponding wind-tunnel value being $1{\cdot}4$. As pointed out in section 3.2, the value as determined from the flight results includes some of the variation of the aircraft profile drag with Reynolds number.

If a correction could be made for this Reynolds number effect the discrepancy between the model and full-scale values of K would be greater. At high Mach number the agreement is quite good (Fig. 12) but it must be remembered that under these conditions the value of K is of doubtful significance since the drag is no longer a linear function of C_L^2.

Conclusions.—(1) It has been shown that measurements of the overall drag of an aircraft in high Mach number dives using the longitudinal accelerometer method can be made to a high standard of accuracy, comparable with that obtainable in level flight measurements. To achieve this, considerable care must be taken to obtain the optimum damping for the accelerometer and continuous records of the acceleration must be taken throughout the dives.

(2) Results obtained in this way on *Meteor IV* showed very good agreement between level-speed and dive measurements, contradicting impressions gained from earlier, less accurate tests.

(3) There was no evidence of the hysteresis effects found in certain other cases, the drag in the dive being independent of whether the Mach number was increasing or decreasing.

(4) Variaton in the engine mass flow over a considerable range made no measurable difference in either the low-speed drag or in the compressibility drag rise.

(5) Close agreement was obtained between flight and wind-tunnel measurements of the increase in the drag coefficient at zero lift with Mach number up to $M = 0{\cdot}82$. The drag coefficient of the *Meteor IV* increased by $0{\cdot}012$ in both the full-scale and model tests on raising the Mach number from $0{\cdot}50$ to $0{\cdot}82$, although the drag rise in the model tests was more gradual and started at a lower Mach number than in flight. This effect may be due to the difference in the boundary-layer flow in the two experiments and for this reason agreement may not be so good for highly tapered or swept wings, where there is a pronounced cross-flow.

(6) The agreement between the flight and wind-tunnel values of K is quite good, especially at high Mach number, but it must be remembered that under these conditions the value of K is of doubtful significance since the drag is no longer a linear function of C_L^2.

REFERENCES

No.	Author	Title, etc.
1	R. Smelt, W. J. Charnley and R. Rose.	Drag and Trim Changes on *Spitfire, Mustang* and *Thunderbolt* in Flight at High Mach Numbers. A.R.C. No. 7424. January, 1944.
2	F. Smith and A. W. Thom.. ..	Note on the use of a Longitudinal Accelerometer for Measuring Aircraft Drag in Flight in the Dive. R.A.E. Tech. Note Aero 1649. June, 1945.
3	F. Smith and A. W. Thom.. ..	Flight Tests on *Meteor I* EE.211 with Lengthened Nacelles. A.R.C. No. 8998. June, 1945.
4	W. J. Charnley	Note on a Method for Correcting for Lag in Aircraft Pitot-Static Lines. R. & M. 2352. September, 1946.
5	W. J. Charnley and I. Fleming ..	The Corrections to be applied to Air-speed Indicator and Altimeter Readings for Position Error and Compressibility Effects. A.R.C. No. 12,365. February, 1949.
6	F. Smith, D. J. Higton and R. H. Plascott.	Flight Tests on the Performance of *Meteor IV*. R. & M. 2446. August, 1946.
7	D. J. Higton, F. Smith and G. Whittle.	Measurements of Tail Loads and Fin Loads by the 'Deflection' Method in Flight at High Mach Numbers on a *Spitfire IX*. A.R.C. No. 9569. February, 1946.
8	J. Y. G. Evans and M. Jones ..	High-Speed Wind-Tunnel Tests on a 1/15 Scale Model of E.18/45 (DH.108) at Mach Numbers up to 0·93. A.R.C. No. 11,493. January, 1948.
9	Sutton	Note on the High-Speed Tunnel Drag Balance For Sting-mounted Models. R.A.E. Technical Memo. No. Aero 35. November, 1948.
10	J. S. Thompson	Present Methods of Applying Blockage Corrections in a Closed Rectangular High-Speed Wind Tunnel. A.R.C. No. 11,385. January, 1948.

APPENDIX I

The Determination of the Thrust of a Jet Engine from Measurements of the Total-Head Pressure and Temperature in the Jet-Pipe in Flight

(a) *Gross Thrust.*—It can be shown that, for a jet-pipe with a fixed final nozzle, the gross thrust depends only on the pressure in the jet-pipe and the pressure after the final nozzle. The pressure in the jet-pipe may be either the static or the total-head pressure. Thus the unit can be calibrated for gross thrust by a pressure point only. The pressure usually measured is the total-head as static measurements are liable to errors due to buckling of the jet-pipe whereas total-head tubes give correct readings even when considerably out of alignment.

The theory of the method is as follows:—The gross thrust is made up of two parts (1) that due to the momentum of the gases and (2) that due to the difference between the pressure at the final nozzle and atmospheric pressure acting on the final area.

If F_G is gross thrust (lb)

F_N nett thrust (lb)

M gas mass flow (lb/sec)

P_f pressure at final nozzle (lb/sq in.)

ρ_f density at final nozzle (lb/cu ft)

T_f temperature at final nozzle (deg C abs.)

V_f velocity at final nozzle (ft/sec)

A_f effective area of final nozzle for calculating gross thrust (sq ft)

A_f' effective area of final nozzle for calculating mass flow (sq ft)

P_e' total-head pressure in the jet-pipe (lb/sq in.)

T_e' total-head temperature in the jet-pipe (deg C abs.)

P_a atmospheric pressure (lb/sq in.)

V_T aircraft true speed (ft/sec)

K_P specific heat at constant pressure (C.H.U./lb/deg C)

J mechanical equivalent of heat (ft lb/C.H.U.)

we have:—

$$F_G = \frac{MV_f}{g} + 144\,(P_f - P_a)\,A_f \cdot$$

Now $M = \rho_f A_f V_f$, $V_f^2 = 2gJK_P(T_e' - T)$ and $\rho_f = \dfrac{144\,P_f}{RT_f}$.

Therefore
$$F_G = \frac{P_f A_f V_f^2}{g} + 144\,(P_f - P_a)\,A_f$$

$$= \frac{144 P_f A_f}{R}\,2JK_P\left[\frac{T_e'}{T_f} - 1\right] + 144\,(P_f - P_a)\,A_f \cdot$$

Now
$$\frac{T_e'}{T_f} = \left(\frac{P_e'}{P_f}\right)^{\frac{\gamma-1}{\gamma}} .$$

Therefore
$$\frac{F_G}{P_a A_f} = 288\,\frac{JK_P}{R}\,\frac{P_f}{P_a}\left[\left(\frac{P_e'}{P_f}\right)^{\frac{\gamma-1}{\gamma}} - 1\right] + 144\left[\frac{P_f}{P_a} - 1\right]$$

$$= 288\,\frac{JK_P}{R}\,\frac{P_e'}{P_a}\left[\left(\frac{P_f}{P_e'}\right)^{\frac{1}{\gamma}} - \frac{P_f}{P_e'}\right] + 144\left[\frac{P_f}{P_a} - 1\right] \cdot$$

Now using the usual values for the gas constants,

i.e., $R = 96{\cdot}4$ ft lb/lb deg C

$K = 0{\cdot}276$ C.H.U./lb/deg C

$\gamma = 1{\cdot}33$

this gives

$$\frac{F_G}{P_a A_f} = 1158\,\frac{P_e'}{P_a}\left[\left(\frac{P_f}{P_e'}\right)^{\frac{1}{\gamma}} - \frac{P_f}{P_e'}\right] + 144\left[\frac{P_f}{P_a} - 1\right] \cdot \quad \ldots \quad \ldots \quad \ldots \quad (1)$$

Before the final nozzle chokes, $P_f = P_a$ and the pressure term is zero. Therefore

$$\frac{F_G}{P_a A_f} = 1158\,\frac{P_e'}{P_a}\left[\left(\frac{P_a}{P_e'}\right)^{\frac{1}{\gamma}} - \frac{P_a}{P_e'}\right] \cdot$$

After the final nozzle chokes, $\dfrac{P_e'}{P_f}$ is a constant and equals $1{\cdot}8505$. The relation between $\dfrac{F_G}{P_a A_f}$ and $\dfrac{P_e'}{P_a}$ then becomes linear.

$$i.e., \quad \frac{F_G}{P_a A_f} = 181{\cdot}05\,\frac{P_e'}{P_a} - 144.$$

The curve for these functions is given in Fig. 13.

(b) *Mass Flow.*—In order to determine the net thrust in flight, we have to subtract the intake momentum loss and for this we require to know the mass flow since,

$$F_N = F_G - \frac{MV_T}{g}\,.$$

It can be shown in a similar manner to the above that, for a fixed final nozzle

$$\frac{M(T_e')^{1/2}}{P_a A_f'} = 144\left(\frac{2gJK_P}{R^2}\right)^{1/2}\left[\frac{P_f}{P_a}\left(\frac{P_e'}{P_f}\right)^{\frac{\gamma-1}{\gamma}}\left(1-\left(\frac{P_f}{P_e'}\right)^{\frac{\gamma-1}{\gamma}}\right)^{1/2}\right] \quad .. \quad .. \quad (2)$$

Thus we can calibrate the unit for mass flow by means of a pressure point and a thermocouple to measure T_e'. Unfortunately, a thermocouple does not measure the full total-head temperature of the gases; if, however, it is assumed that it measures a constant proportion (k say) of the dynamic temperature rise, we have:—

$$T_{e\,\text{indicated}}' = T_e + k(T_e' - T_e) \quad .. \quad .. \quad .. \quad .. \quad .. \quad .. \quad (3)$$

where T_e is the static temperature at the measuring section.

Equation (3) can be written

$$\frac{T_{e\,\text{ind.}}'}{T_e'} = k + (1-k)\frac{T_e}{T_e'} = k + (1-k)\left(\frac{P_e}{P_e'}\right)^{\frac{\gamma-1}{\gamma}} \quad .. \quad .. \quad .. \quad .. \quad (4)$$

where P_e is the static pressure at the measuring section. If we assume that the total-head pressure in the jet-pipe (P_e') remains constant up to the final nozzle, we can apply Bernoulli's equation to the conditions at the measuring section and at the final nozzle to obtain expressions for the velocities at the measuring section and the final nozzle (V_e and V_f respectively), *viz:*—

$$\tfrac{1}{2}v_e^2 = \frac{\gamma}{\gamma-1}\left(\frac{P_e'}{\rho_e'} - \frac{P_e}{\rho_e}\right) = \frac{\gamma}{\gamma-1}\cdot\frac{P_e'}{\rho_e'}\left(1 - \frac{P_e}{P_e'}\,\frac{\rho_e'}{\rho_e}\right) = \frac{\gamma}{\gamma-1}\cdot\frac{P_e'}{\rho_e'}\left[1-\left(\frac{P_e}{P_e'}\right)^{\frac{\gamma-1}{\gamma}}\right]$$

where ρ_e' is the density corresponding to conditions of rest,

and ρ_e is the density at the measuring section.

Similarly,

$$\tfrac{1}{2}v_f^2 = \frac{\gamma}{\gamma-1}\,\frac{P_e'}{\rho_e'}\left[1-\left(\frac{P_f}{P_e'}\right)^{\frac{\gamma-1}{\gamma}}\right].$$

Now from continuity,

$$\rho_e A_e v_e = \rho_f A_f' v_f$$

where A_e is the effective cross-sectional area at the measuring section,

or $$\tfrac{1}{2}v_e^2\rho_e^2 A_e^2 = \tfrac{1}{2}v_f^2\rho_f^2 A_f'^2$$

or $$\frac{\gamma}{\gamma-1}\,A_e^2\rho_e^2\,\frac{P_e'}{\rho_e'}\left[1-\left(\frac{P_e}{P_e'}\right)^{\frac{\gamma-1}{\gamma}}\right] = \frac{\gamma}{\gamma-1}\,A_f'^2\rho_f^2\,\frac{P_e'}{\rho_e'}\left[1-\left(\frac{P_f}{P_e'}\right)^{\frac{\gamma-1}{\gamma}}\right]$$

which, after substituting $\frac{\rho_e'}{\rho_e} = \left(\frac{P_e'}{P_e}\right)^{\frac{1}{\gamma}}$ and simplifying, becomes:—

$$\left(\frac{P_e}{P_e'}\right)^{\frac{2}{\gamma}}\left[1 - \left(\frac{P_e}{P_e'}\right)^{\frac{\gamma-1}{\gamma}}\right] = \left(\frac{A_f'}{A_e}\right)^2\left(\frac{P_f}{P_e'}\right)^{\frac{2}{\gamma}}\left[1 - \left(\frac{P_f}{P_e'}\right)^{\frac{\gamma-1}{\gamma}}\right] \cdot \quad .. \quad .. \quad (5)$$

From this equation, used in conjunction with (4) and (2), curves for $M\sqrt{T_e'_{\text{ind}}}/P_a A_f$ against P_e'/P_a for different values of A_e/A_f' can be drawn and these are shown in Fig. 14 for three values of A_e/A_f' using the value $k = 0{\cdot}6$. It will be seen that the difference between the curves for values of A_e/A_f' of $1{\cdot}0$ and infinity amounts to only about 3 per cent. Thus the error in net thrust introduced by neglecting the inaccuracy of the thermocouple is only of the order of $1\frac{1}{2}$ per cent, as the intake momentum loss is usually about half of the net thrust at speeds around the above normal cruising.

It should be remembered that the mass flow measured is the total gas mass flow, whereas that used in calculating the intake momentum loss is only the air mass flow. The measured values should be corrected therefore for the fuel flow; it is sufficiently accurate to use the maker's specification figures for this if no fuel flow measurements are made.

It should be noted that the value of k used in Fig. 14 ($0{\cdot}6$) applies to thermocouples that are totally sheathed. In thermocouples, such as the Type ' B ' Pyrometer, which is now extensively used in jet-propulsion engines, in which the gas is reduced nearly to rest around the thermocouple junction the value of k is very nearly unity. From equation (4) it will be seen that the thermocouple will read the correct temperature if k is unity or if $P_e/P_e' = 1$. From equation (5) it is found that $P_e/P_e' = 1{\cdot}0$ if $A_e/A_f' = \infty$. Hence the top curve in Fig. 14 can be used for all mass flow calculations if the k for the thermocouple used is unity.

APPENDIX II

The Longitudinal Accelerometer Method of Measuring the Overall Drag of an Aircraft in Non-steady Flight

The theory of this method of drag measurement for the single case, where the longitudinal accelerometer is directed along the flight path of the aircraft, is given correctly in Ref. 2. However, in general the accelerometer is not directed along the flight path and corrections have therefore to be applied for this. Further corrections have to be applied since the thrust line is not along the line of flight, and the axis of the normal accelerometer is not perpendicular to the line of flight. It is this general case, where no assumptions are made concerning the directions of the accelerometers with respect to the flight path, that is considered here. It is assumed that the accelerometers are mounted at right-angles to each other.

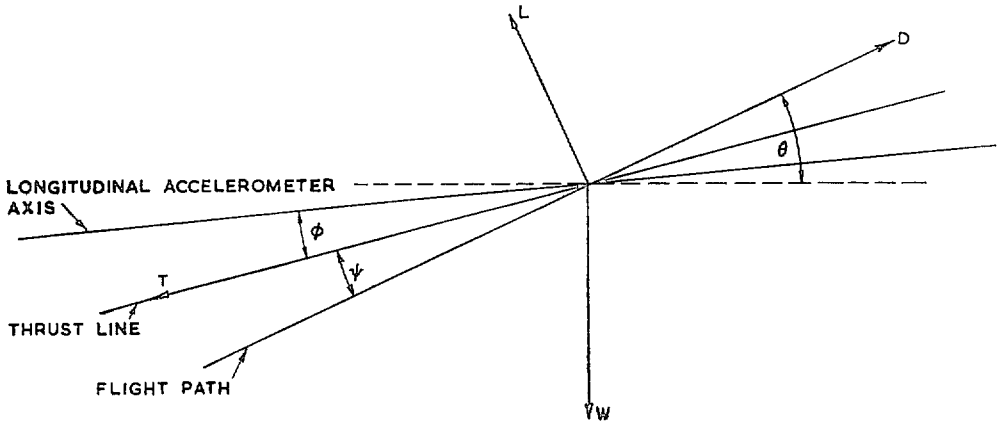

If W is weight of aircraft

L lift on aircraft

D overall drag of aircraft

T thrust on aircraft

θ angle of flight path to horizontal

ϕ angle between thrust line and longitudinal accelerometer axis

ψ angle between thrust line and flight path

W_l weight of longitudinal accelerometer weight

W_n weight of normal accelerometer weight

then,

acceleration of aircraft centre of gravity along a line parallel to the longitudinal accelerometer axis is Ag say,

$$= \frac{g}{W} [W \sin (\theta - \phi - \psi) + T \cos \phi - D \cos (\phi + \psi) + L \sin (\phi + \psi)].$$

Therefore $A = \sin (\theta - \phi - \psi) + \frac{T}{W} \cos \phi - \frac{D}{W} \cos (\phi + \psi) + \frac{L}{W} \sin (\phi + \psi)$.

Acceleration of aircraft c.g. along a line perpendicular to the longitudinal accelerometer axis is Ng say,

$$= \frac{g}{W} [W \cos (\theta - \phi - \psi) + T \sin \phi - D \sin (\phi + \psi) - L \cos (\phi + \psi)].$$

Therefore $N = \cos (\theta - \phi - \psi) + \frac{T}{W} \sin \phi - \frac{D}{W} \sin (\phi + \psi) - \frac{L}{W} \cos (\phi + \psi)$.

Acceleration of longitudinal accelerometer weight along longitudinal accelerometer axis, if unrestrained is lg, say,

$$= \frac{g}{W_l} W_l \sin (\theta - \phi - \psi).$$

Therefore $l = \sin (\theta - \phi - \psi)$.

Acceleration of normal accelerometer weight along normal accelerometer axis, if unrestrained is ng, say,

$$= \frac{g}{W_n} W_n \cos (\theta - \phi - \psi).$$

Therefore $n = \cos (\theta - \phi - \psi)$.

Therefore reading of longitudinal accelerometer in g units is R, say

$$= l - A.$$

Therefore $R = \frac{D}{W}\cos(\phi+\psi) - \frac{T}{W}\cos\phi - \frac{L}{W}\sin(\phi+\psi)$. .. .. .. (1)

Reading of normal accelerometer in g units is Q, say

$$= n - N.$$

Therefore $Q = \frac{L}{W}\cos(\phi+\psi) + \frac{D}{W}\sin(\phi+\psi) - \frac{T}{W}\sin\phi$ . .. . (2)

From (2)

$$\frac{L}{W} = \left[Q + \frac{T}{W}\sin\phi - \frac{D}{W}\sin(\phi+\psi)\right]\sec(\phi+\psi).$$

Substituting this in (1) gives,

$$R = \frac{D}{W}\cos(\phi+\psi) - \frac{T}{W}\cos\phi - Q\tan(\phi+\psi) - \frac{T}{W}\sin\phi\tan(\phi+\psi)$$

$$+ \frac{D}{W}\sin(\phi+\psi)\tan(\phi+\psi)$$

or

$$R + Q\tan(\phi+\psi) = \left[\frac{D}{W} - \frac{T}{W}\cos\psi\right]\sec(\phi+\psi)$$

or approximately

$$R + Q(\phi+\psi) = \left[\frac{D-T}{W} + \frac{T\psi^2}{2W}\right]\left[1 + \frac{(\phi+\psi)^2}{2}\right]$$

$$= \left(\frac{D-T}{W}\right) + \left(\frac{D-T}{W}\right)\frac{(\phi+\psi)^2}{2} + \frac{T\psi^2}{2W}$$

which becomes,

$$\frac{D-T}{W} = R + Q(\phi+\psi) - \frac{R}{2}(\phi+\psi)^2 - \frac{T\psi^2}{2W} \quad .. .. .. (3)$$

During the tests described in this report, it was found that the last two terms on the right-hand side of equation (3) were negligible in comparison with the other two. Hence for these tests the expression used was,

$$\frac{D-T}{W} = R + Q(\phi+\psi).$$

In this expression, it is necessary to know the incidence of the aircraft throughout the tests. This was obtained from a lift carpet from high-speed wind-tunnel tests. Hence having calculated the thrust by the method described in Appendix I, and estimated the weight of the aircraft the overall drag was obtained from the readings of the two accelerometers.

The profile drag is then obtained by subtracting the induced drag which must be corrected for any changes in lift coefficient due to normal acceleration.

TABLE I

Details of 'Meteor' IV EE. 454 *and* VT. 108

	EE.454	VT.108
Wing area (sq ft)	374	350
Wing setting to body datum (degrees)	1·0	1·0
Wing section	EC 1240/0640 EC 0940/0640	(root) (tip)
Span	43 ft 0 in.	37 ft 4 in.
Aspect ratio	4·95	3·98
Taper ratio	3 : 1	2·2 : 1
Tailplane area (sq ft)	66	66
Tailplane setting (degrees to W.R.C.)	$-\frac{1}{2}$ deg	0 deg
Aerodynamic mean chord	109·5	116·6
All-up weight (lb)	13,810	14,720
C.G. position at full weight (per cent A.M.C.) ..	30·0	27·5
Fuel capacity (gall)	325	325

The model tested in the wind tunnel was 1/12 scale of *Meteor* EE.454.

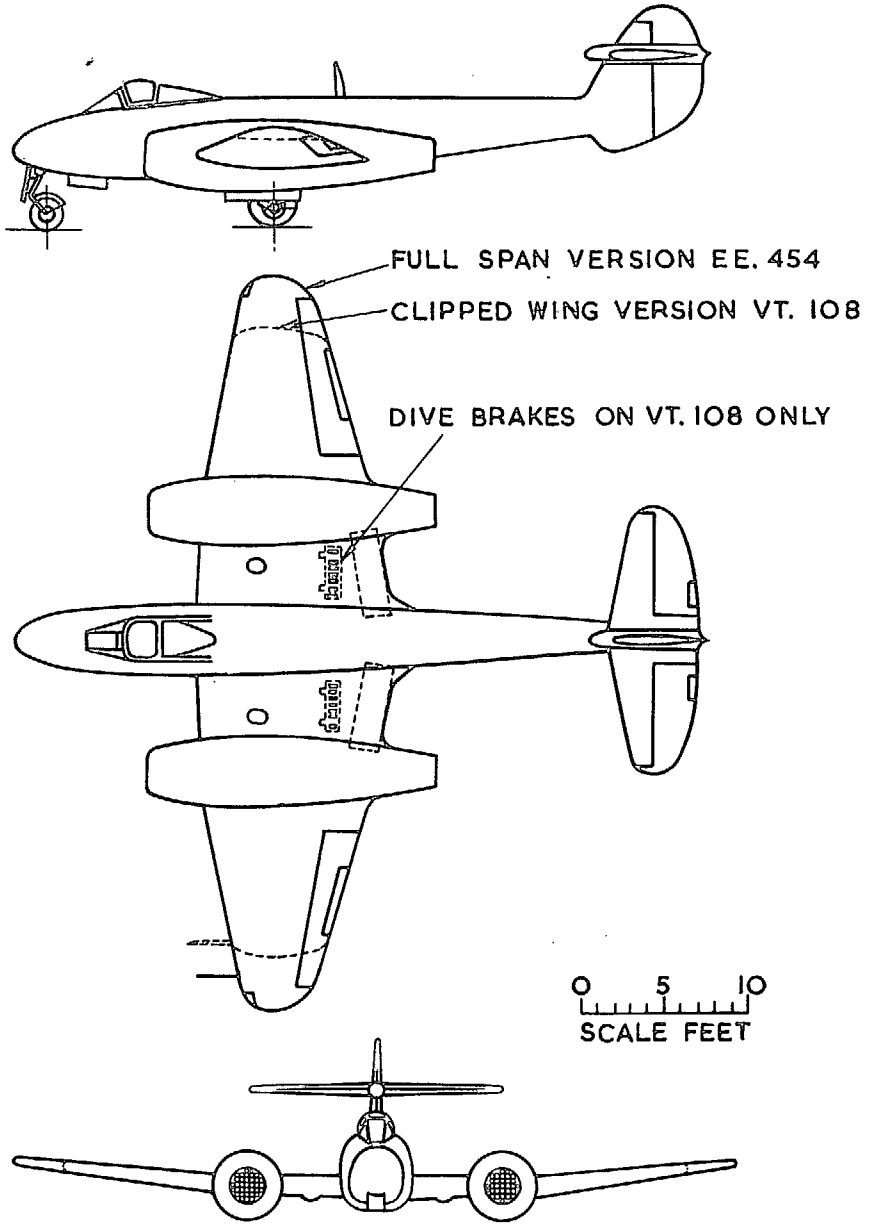

FIG. 1. *Meteor IV*. General arrangement of aircraft.

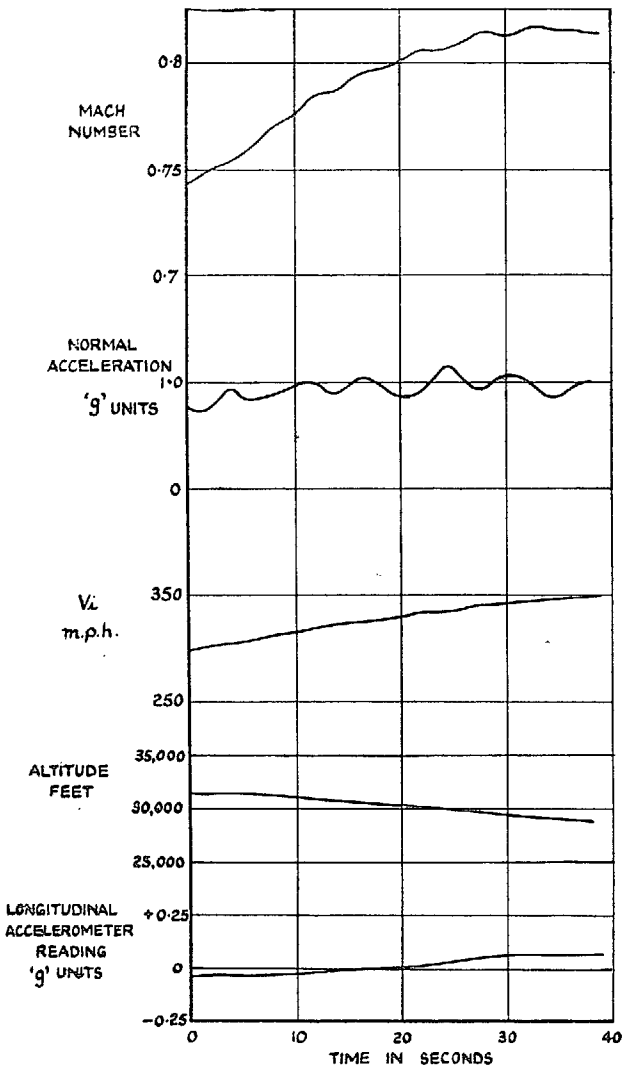

FIG. 2a. *Meteor IV* EE.454. Typical time history of a dive at 14,000 r.p.m.

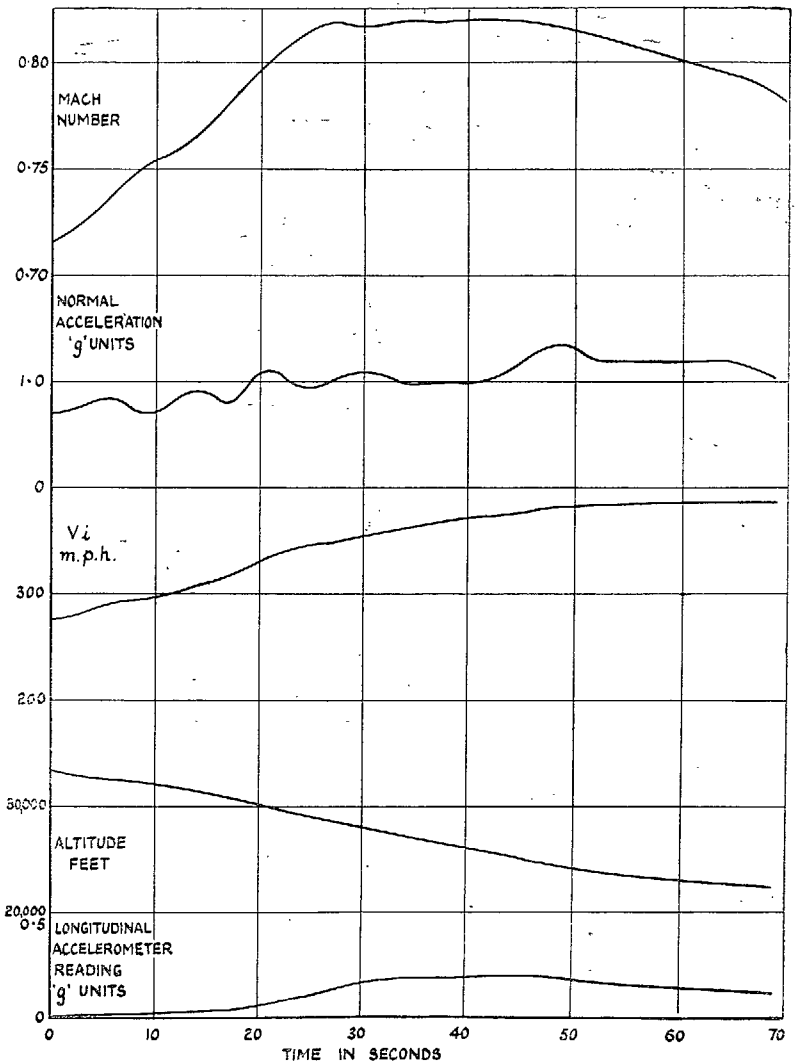

FIG. 2b. *Meteor IV* EE.454. Typical time history of a dive at 12,000 r.p.m.

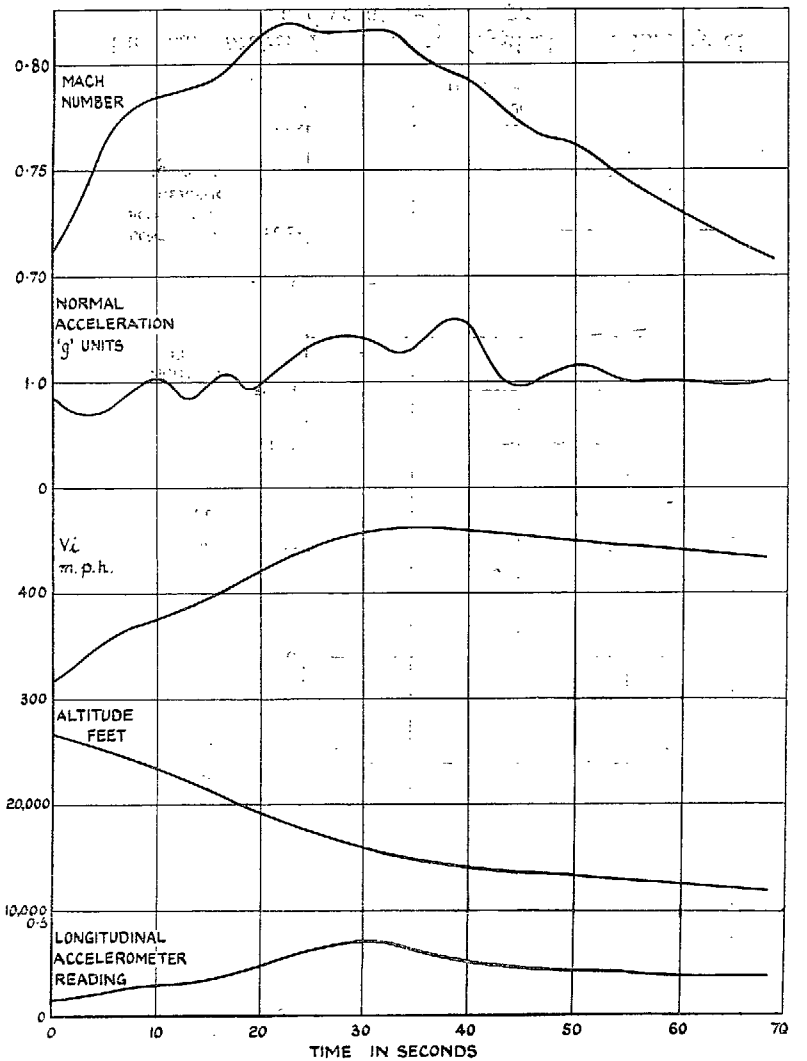

FIG. 2c. *Meteor IV* EE.454. Typical time history of a dive at 10,000 r.p.m.

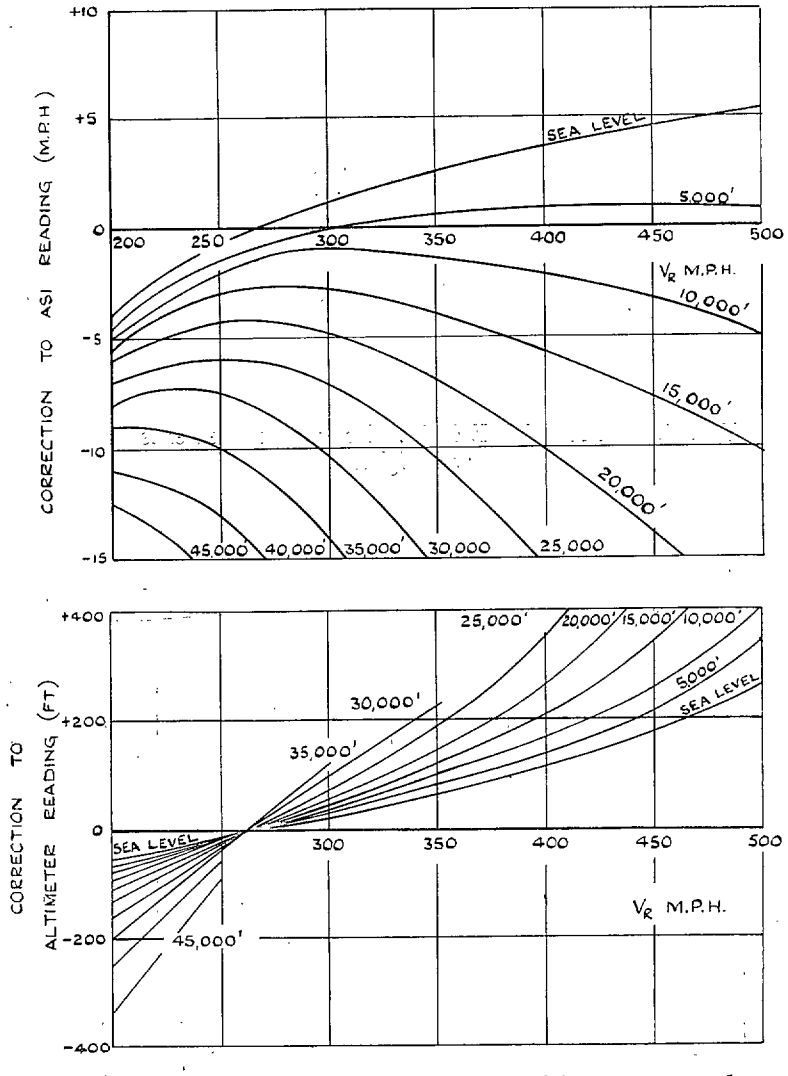

FIG. 3. *Meteor IV* VT.108. Position error and compressibility correction to indicated airspeed and altitude.

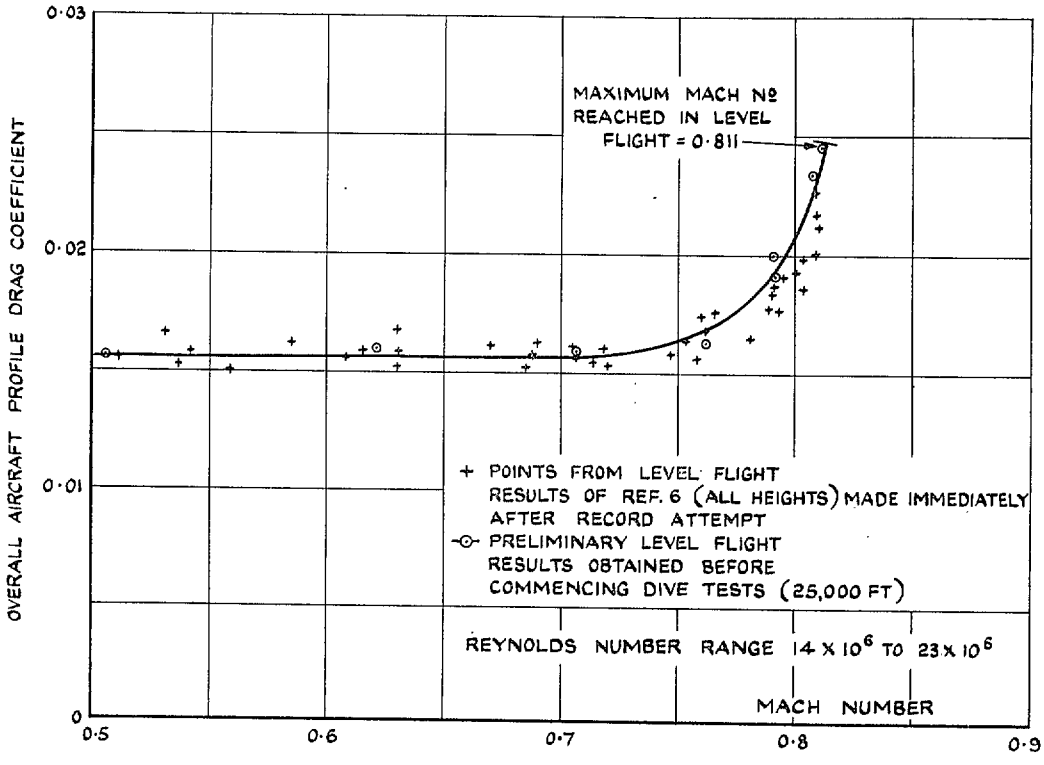

FIG. 4. *Meteor IV* EE.454. Drag measurements in level flight.

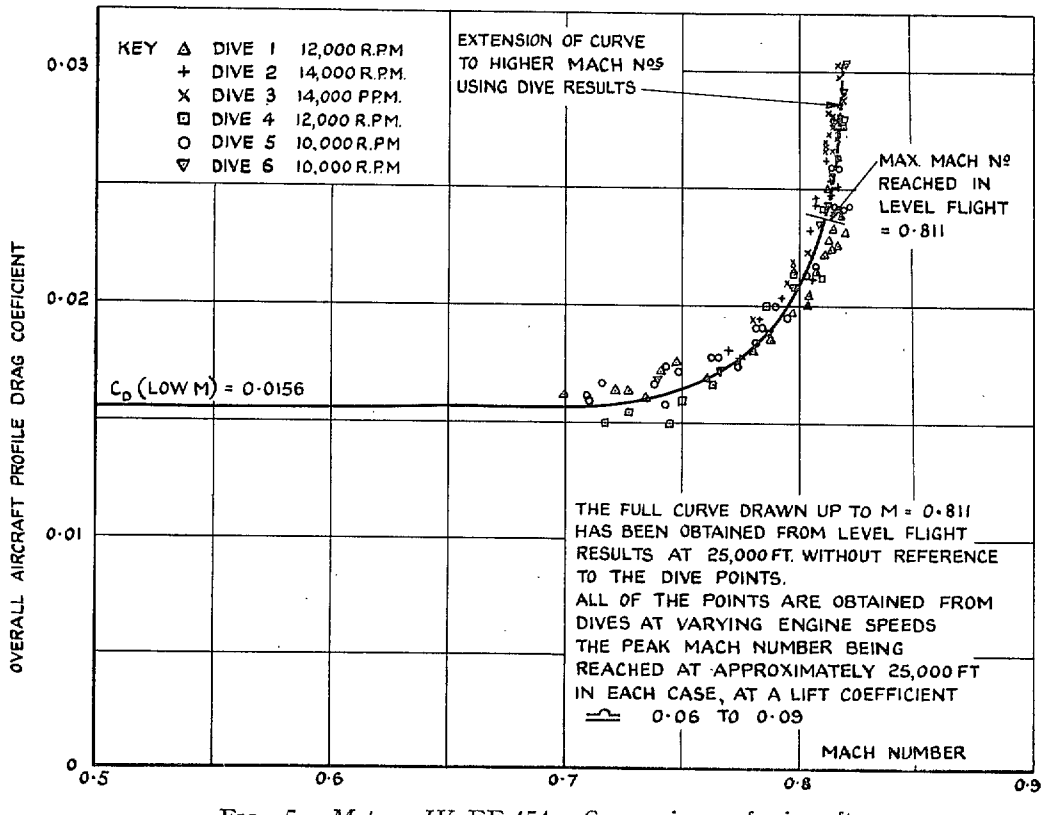

FIG. 5. *Meteor IV* EE.454. Comparison of aircraft drag measured in level flight and in dives.

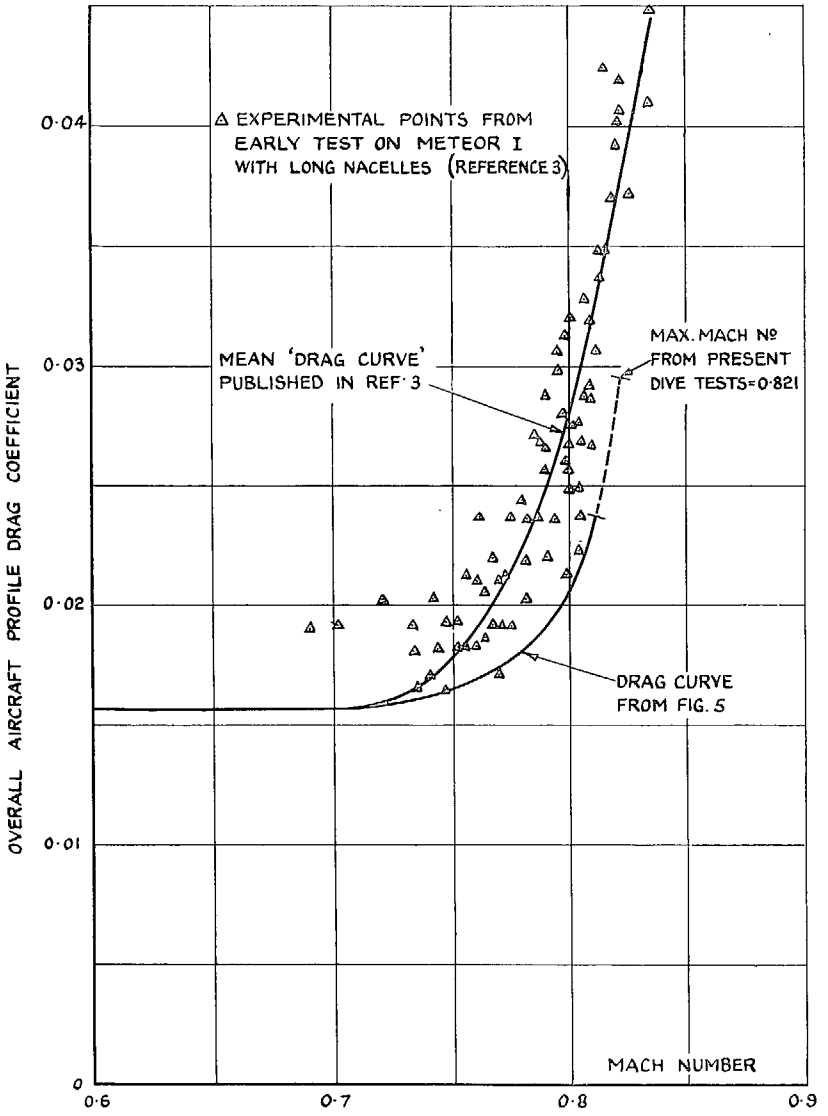

FIG. 6. *Meteor IV* EE.454. Comparison between early results from *Meteor I* EE.211 with long nacelles and present results from *Meteor IV* EE.454.

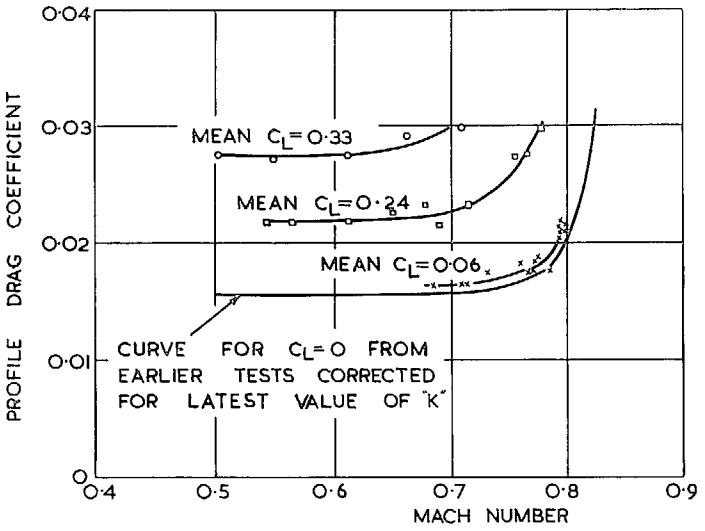

FIG. 7. Drag of *Meteor IV* VT.108. Flight results compared with drag measured in earlier flight tests corrected to latest value of k.

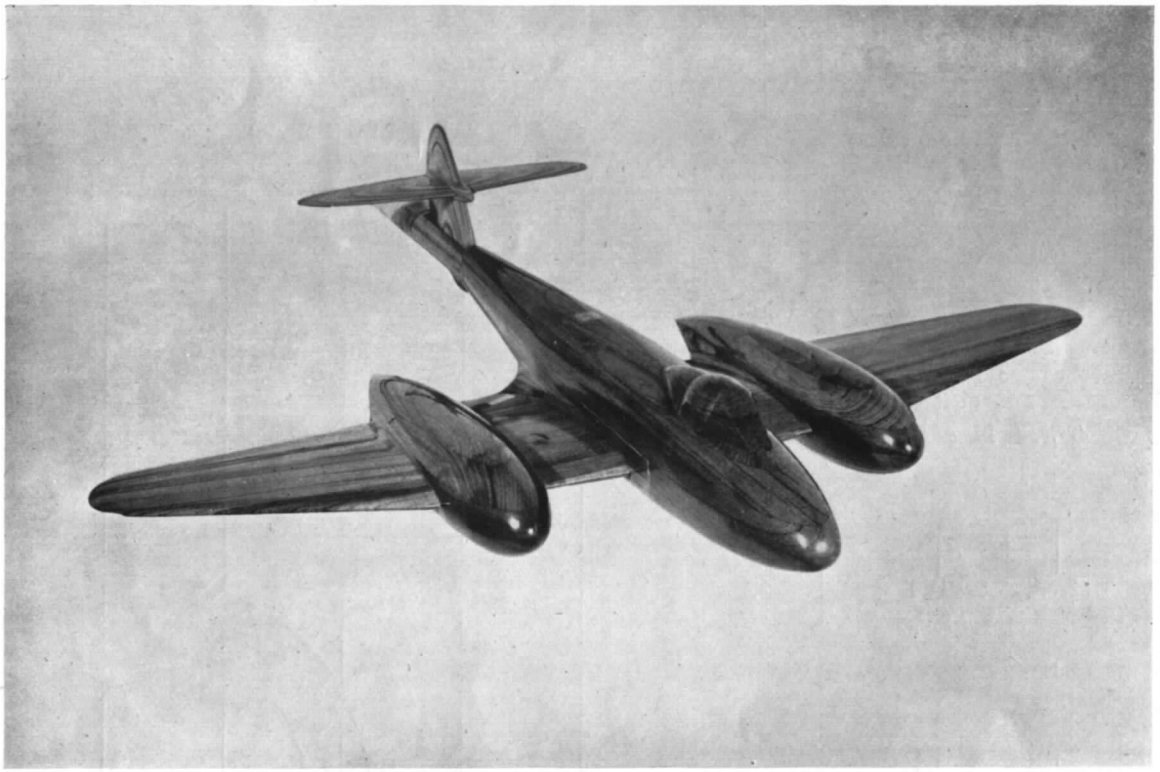

FIG. 8. 1/12th Scale model of *Meteor IV* EE.454.

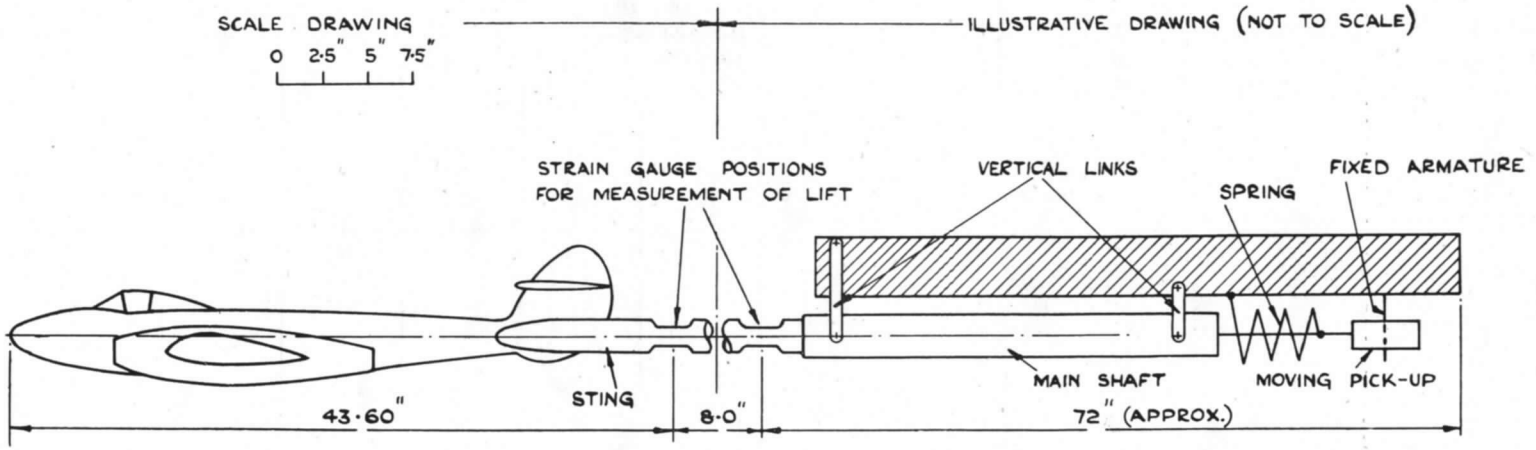

FIG 9. Schematic drawing of installation in wind tunnel showing method of drag measurement.

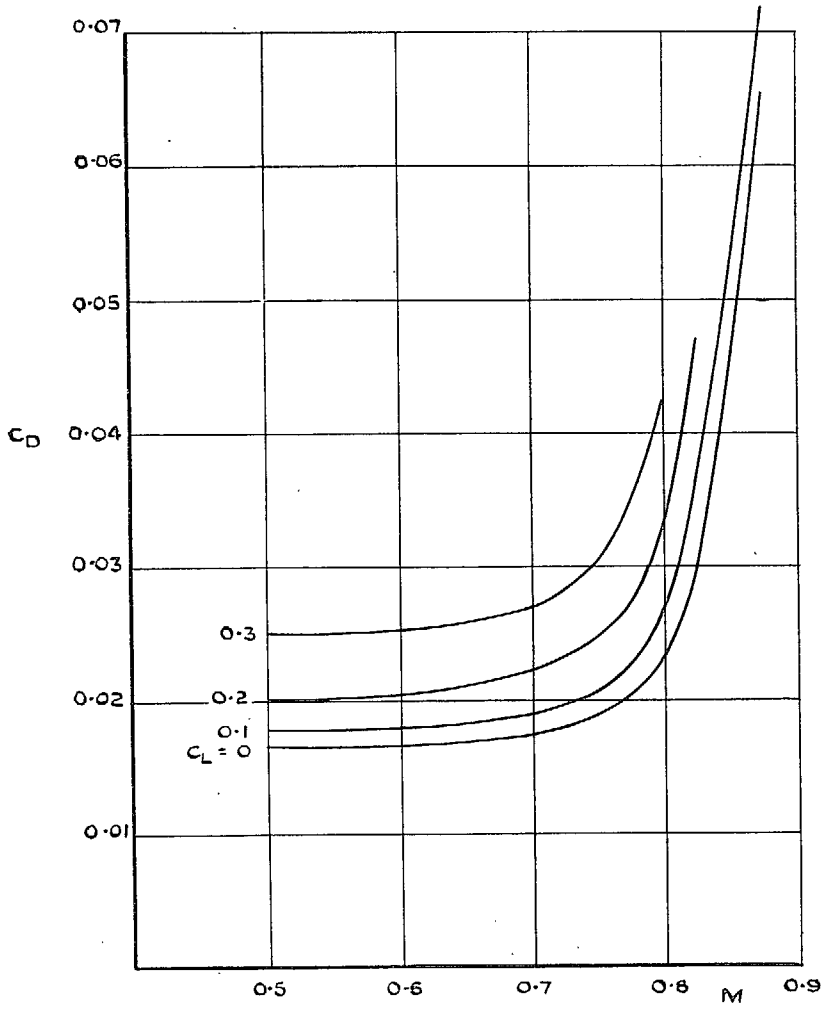

FIG. 10. Drag of 1/12th scale model of *Meteor IV* EE.454 at various lift coefficients.

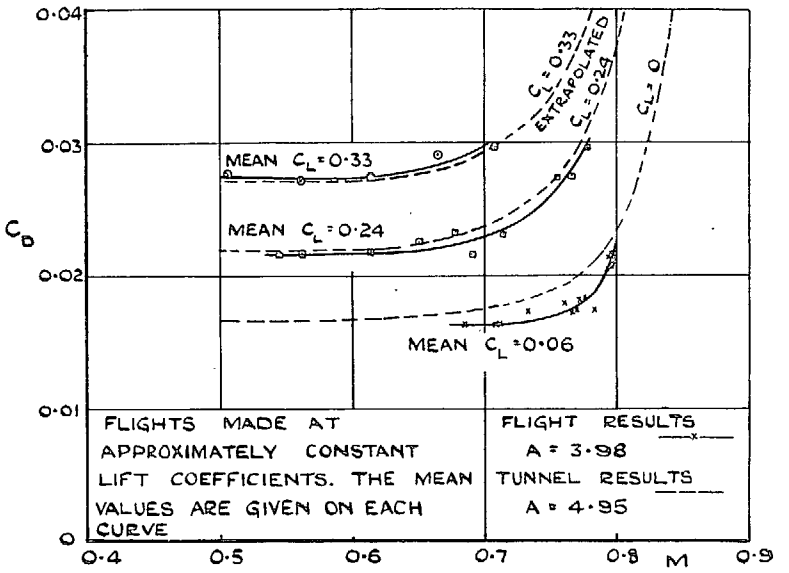

FIG. 11. Drag of *Meteor IV*. (VT.108 in flight and EE.454 model in wind tunnel.)

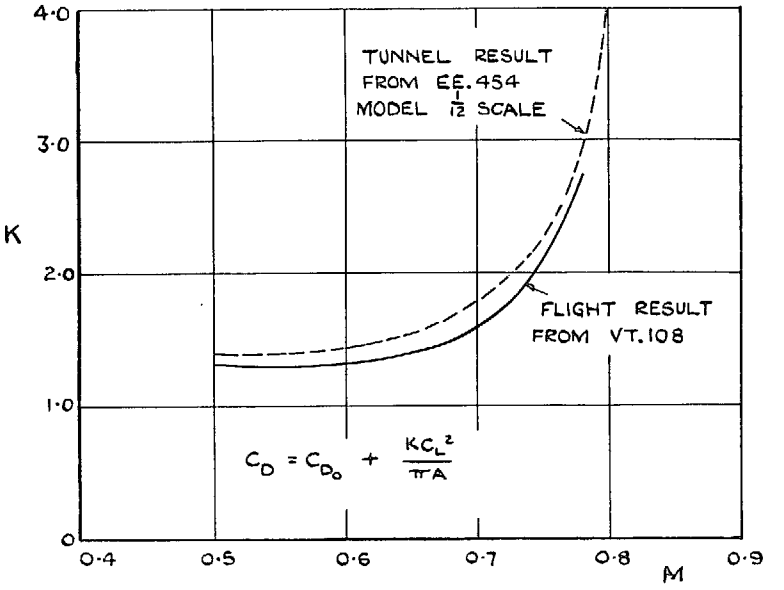

FIG. 12. Factor K for *Meteor IV*. (VT.108 in flight and EE.454 model in wind tunnel).

(23113) Wt. 15-680 K9 7/53 F. M. & S.

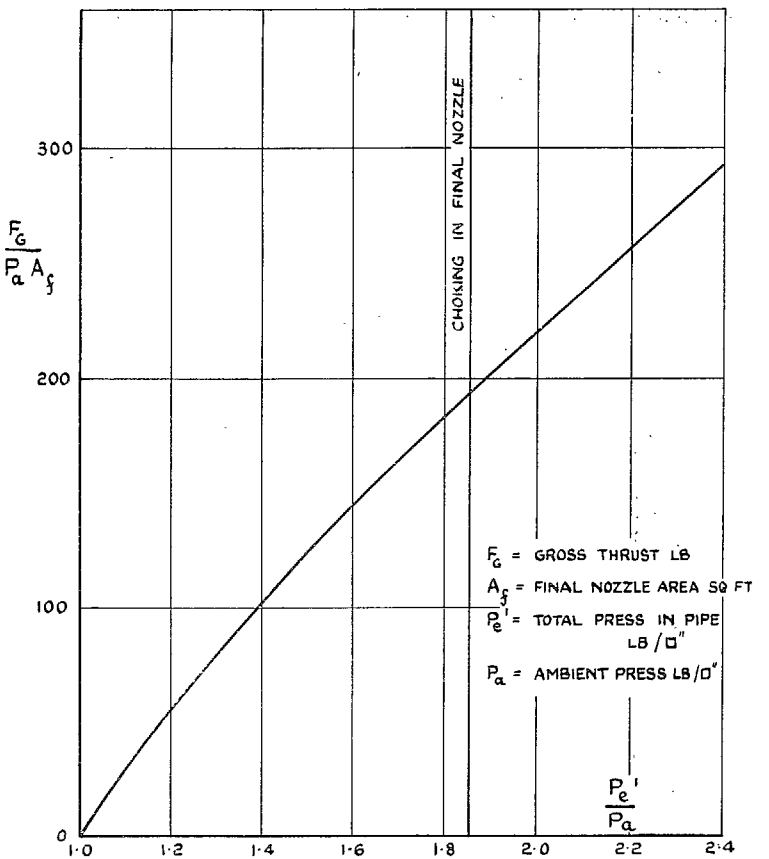

FIG. 13. Curve of $\frac{\text{gross thrust}}{P_a A_f}$ against $\frac{P_{e'}}{P_a}$ for use in conjunction with Appendix I to calculate engine gross thrust.

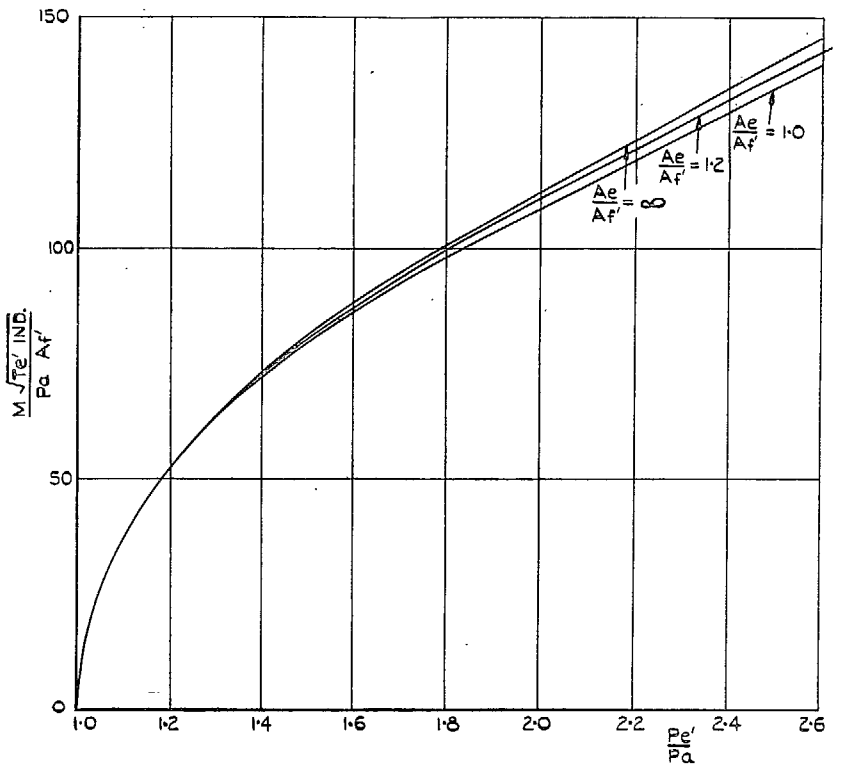

FIG. 14. Curve of $\frac{\text{mass flow } (T_{e'\text{ind.}})^{1/2'}}{P_a A_f'}$ against $\frac{P_e'}{P_a}$ for use in conjunction with Appendix I to calculate engine mass flow.

PRINTED IN GREAT BRITAIN

Publications of the Aeronautical Research Council

ANNUAL TECHNICAL REPORTS OF THE AERONAUTICAL RESEARCH COUNCIL (BOUND VOLUMES)

1936 Vol. I. Aerodynamics General, Performance, Airscrews, Flutter and Spinning. 40*s.* (40*s.* 9*d.*)
Vol. II. Stability and Control, Structures, Seaplanes, Engines, etc. 50*s.* (50*s.* 10*d.*)

1937 Vol. I. Aerodynamics General, Performance, Airscrews, Flutter and Spinning. 40*s.* (40*s.* 10*d.*)
Vol. II. Stability and Control, Structures, Seaplanes, Engines, etc. 60*s.* (61*s.*)

1938 Vol. I. Aerodynamics General, Performance, Airscrews. 50*s.* (51*s.*)
Vol. II. Stability and Control, Flutter, Structures, Seaplanes, Wind Tunnels, Materials. 30*s.* (30*s.* 9*d.*)

1939 Vol. I. Aerodynamics General, Performance, Airscrews, Engines. 50*s.* (50*s.* 11*d.*)
Vol. II. Stability and Control, Flutter and Vibration, Instruments, Structures, Seaplanes, etc. 63*s.* (64*s.* 2*d.*)

1940 Aero and Hydrodynamics, Aerofoils, Airscrews, Engines, Flutter, Icing, Stability and Control, Structures, and a miscellaneous section. 50*s.* (51*s.*)

1941 Aero and Hydrodynamics, Aerofoils, Airscrews, Engines, Flutter, Stability and Control, Structures. 63*s.* (64*s.* 2*d.*)

1942 Vol. I. Aero and Hydrodynamics, Aerofoils, Airscrews, Engines. 75*s.* (76*s.* 3*d.*)
Vol. II. Noise, Parachutes, Stability and Control, Structures, Vibration, Wind Tunnels. 47*s.* 6*d.* (48*s.* 5*d.*)

1943 Vol. I. (In the press.)
Vol. II. (In the press.)

ANNUAL REPORTS OF THE AERONAUTICAL RESEARCH COUNCIL—

1933-34 1*s.* 6*d.* (1*s.* 8*d.*)
1934-35 1*s.* 6*d.* (1*s.* 8*d.*)
April 1, 1935 to Dec. 31, 1936. 4*s.* (4*s.* 4*d.*)
1937 2*s.* (2*s.* 2*d.*)
1938 1*s.* 6*d.* (1*s.* 8*d.*)
1939-48 3*s.* (3*s.* 2*d.*)

INDEX TO ALL REPORTS AND MEMORANDA PUBLISHED IN THE ANNUAL TECHNICAL REPORTS AND SEPARATELY—

April, 1950 - - - - - R. & M. No. 2600. 2*s.* 6*d.* (2*s.* 7½*d.*)

AUTHOR INDEX TO ALL REPORTS AND MEMORANDA OF THE AERONAUTICAL RESEARCH COUNCIL—

1909-1949 - - - - - R. & M. No. 2570. 15*s.* (15*s.* 3*d.*)

INDEXES TO THE TECHNICAL REPORTS OF THE AERONAUTICAL RESEARCH COUNCIL—

December 1, 1936—June 30, 1939. R. & M. No. 1850. 1*s.* 3*d.* (1*s.* 4½*d.*)
July 1, 1939—June 30, 1945. R. & M. No. 1950. 1*s.* (1*s.* 1½*d.*)
July 1, 1945—June 30, 1946. R. & M. No. 2050. 1*s.* (1*s.* 1½*d.*)
July 1, 1946—December 31, 1946. R. & M. No. 2150. 1*s.* 3*d.* (1*s.* 4½*d.*)
January 1, 1947—June 30, 1947. R. & M. No. 2250. 1*s.* 3*d.* (1*s.* 4½*d.*)
July, 1951. - - - - - R. & M. No. 2350. 1*s.* 9*d.* (1*s.* 10½*d.*)

Prices in brackets include postage.

Obtainable from

HER MAJESTY'S STATIONERY OFFICE

York House, Kingsway, London, W.C.2; 423 Oxford Street, London, W.1 (Post Orders: P.O. Box 569, London, S.E.1); 13a Castle Street, Edinburgh 2; 39 King Street, Manchester 2; 2 Edmund Street, Birmingham 3; 1 St. Andrew's Crescent, Cardiff; Tower Lane, Bristol 1; 80 Chichester Street, Belfast or through any bookseller.